Integrated Optimal Design of Heterogeneous Electrical Energetic Systems using Multiobjective Genetic Algorithms

Bruno Sareni, Jérémi Régnier, Xavier Roboam

Integrated Optimal Design of Heterogeneous Electrical Energetic Systems using Multiobjective Genetic Algorithms

B. Sareni* J. Régnier* and X. Roboam*

Abstract *–This paper explores the use of Multiobjective Genetic algorithms (MOGAs) for the Integrated Optimal Design (IOD) of complex heterogeneous power systems in electrical engineering. IOD consists in simultaneously optimizing architecture, structural characteristics, sizing of the constitutive elements and energy management in complex systems. An example of IOD is given in the paper through the case of a traction device for electric vehicles. It is shown that MOGAs lead on the one hand to the optimization of given objectives for performance improvement and on the other hand, provide a better understanding of system behavior through the analysis of Pareto-optimal solutions.*

Keywords*: Genetic Algorithms, Multiobjective Optimization, Integrated Optimal Design, Power Systems, Electric Vehicles.*

I. Introduction

The determination of innovative industrial solutions for complex energetic systems requires the improvement of design tools and methodologies. In particular, systems should be considered globally ensure optimal performance. Indeed the local optimization of system elements independently taken, does not guarantee the optimality of the whole. In most cases, couplings existing between the elements directly affect global efficiency. On the other hand, several aspects have to be considered at the same level in the design process such as the choice of the system architecture, the element sizing and the energy management strategy. These features are strongly coupled to global performance.

Integrated Optimal Design (IOD) in electrical engineering aims at simultaneously optimizing the architecture, the element sizing and the energy management in heterogeneous power systems. IOD necessary leads to complex mixed variable optimization problems with multiple constraints and objectives. Classical optimization methodologies used in the past to solve this kind of problems have shown strong limitations. Today, MultiObjective Genetic Algorithms (MOGAs) offer interesting insight in the context of IOD and global optimization. In this paper, we illustrate the application of MOGAs to a typical example of IOD which consists in determining optimal traction devices for electric vehicles (EVs).

The paper is organized as follows. In the first part, the concept of IOD is introduced and the main features are given. Secondly, a brief overview of MOGAs is carried out and their adaptation to the IOD context is discussed. Finally, the last part is devoted to the optimization of traction devices for EVs capable of fulfilling urban or road driving cycles.

II. Integrated Optimal Design in Electrical Engineering

II.1. The issue of Energetic System Design

The design of electrical energetic systems represents a societal challenge. The increasing demands in terms of energetic needs and efficiency requirements for energetic systems have to be fulfilled. Instead of current devices which are generally oversized in relation to their power needs, innovative systems should now be designed as accurately as possible to avoid energetic wastes. The difficulties related to the optimization of such systems are related to several features:

- these systems are characterized by a high level of complexity, being composed of multiple subsystems whose architecture and dimensioning have to be determined to reach optimal performance
- these systems are strongly heterogeneous, multi-domain composed of elements with different physical types (electric, mechanic, thermal) and multi-time scaled models. This leads the designer to raise the question of the level of representation for the system elements and the corresponding model types (analytical, numerical such as algebra-differential equations or finite element models) in relation to a compromise associated with accuracy and computational costs.

Because of these main difficulties, the design process was simplified in the past using a sequential approach consisting in:

- finding the most suitable system architecture
- optimizing element sizing
- finding an optimal energy management strategy for the system

However, as indicated in Fig. 1, couplings existing between these factors and their influence on global

system efficiency require evolution toward a global optimization approach. We name this approach as Integrated Optimal Design (IOD) since it aims at concurrently optimizing architecture, element sizing and energy management in a given system.

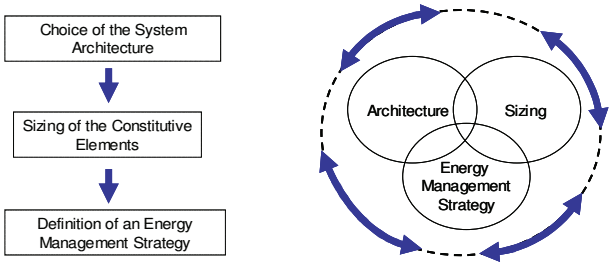

Fig. 1. Design Process Approaches.
(a) Sequential Design (b) Integrated Optimal Design

II.2. The Electric Vehicle Example

"Pure" electric vehicles (PEV's) are typical examples of complex heterogeneous energetic systems. They are composed of several elements including the frame and the electrical traction device, itself constituted by an energy supply (battery) and a static power converter which controls the electrical motor. Power is transferred to the wheel through a reducer and a mechanical transmission line. The synoptic of the traction system of a PEV is given in Fig. 2.

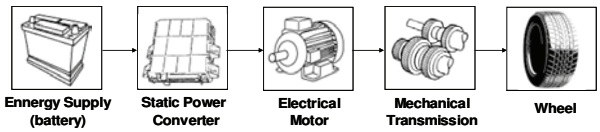

Fig. 2. Synoptic of the traction system of a "pure" electric vehicle

Note that the architecture of the electrical traction device can be more complicated in the case of hybrid vehicles (i.e. vehicles with multiple energy supplies) and multi-motor solutions (i.e. one motor per wheel for example).

The electrical vehicle designer is confronted with choices related to traction device architecture, element type and size (i.e. batteries, static converters, motors). These choices are strongly linked to geometrical and mechanical characteristics of the vehicle (i.e. frame mass and volume, drag coefficient) and to its capacity to fulfill typical driving cycles (i.e. urban, road or highway cycles). Fig. 3 illustrates some coupling elements in a PEV.

II.3. Integrated Optimal Design

The main difficulty of the IOD approach resides in the choice of a suitable level of description for each element in the system. Models with low description levels can lead to an inaccurate system behavior and/or will not offer sufficient degrees of freedom for the objective improvement and the design constraint fulfillment. On the other hand, models with high description levels will be of greater complexity and will considerably affect the computational time and/or the difficulty to identify relevant design variables in the optimization process. A good compromise between accuracy and complexity should be done which often implies the exploitation of *a priori* information and knowledge by the designer and the specialists of each element in the system.

Moreover, the corresponding optimization problems resulting from this approach are rather complex. In particular, they are usually characterized by:

- an important number of design variables which can be discrete (combinatorial parameters related to system architecture, constitutive elements or materials) and/or continuous (sizing parameters and energetic variables).
- multiple constraints intrinsic to each subsystem or related to the associative compatibility between elements in the system.
- several objectives to optimize, typically energetic criteria (efficiency, energetic consumption, energetic losses), sizing factors (volume, mass) or economic costs.

In this context, Multiobjective Genetic Algorithms (MOGAs) seems to be well suited to solve this kind of problems.

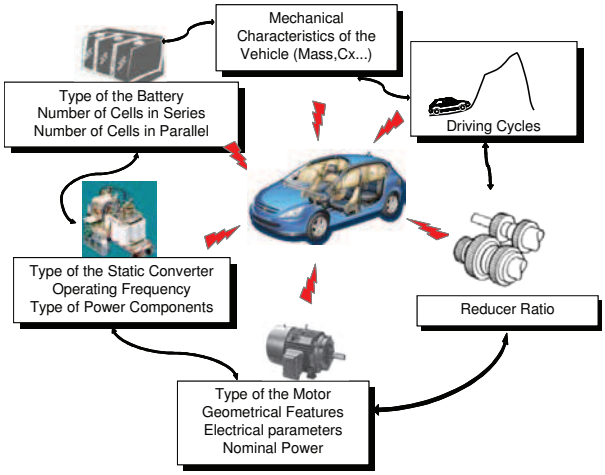

Fig. 3. Example of coupling elements in a PEV

III. Multiobjective Optimization with Genetic Algorithms

III.1. Multiobjective Optimization Problems and Pareto Optimality

Multiobjective optimization seeks to simultaneously minimize n objectives where each of them is a function of a vector $\mathbf{X}$ of m parameters (decision variables or design variables). These parameters may also be subject to k inequality constraints, so that the optimization problem may be expressed as:

$$\begin{aligned} &\text{Minimize} \quad f(\mathbf{X}) = (f_1(\mathbf{X}), f_2(\mathbf{X}), \cdots, f_n(\mathbf{X})) \\ &\text{subject to} \quad g_i(\mathbf{X}) \le 0 \quad \text{for } i = 1...k \end{aligned} \tag{1}$$

For this kind of problem, objectives typically conflict with each other. Thus, in most cases, it is impossible to obtain the global minimum at the same point for all objectives. Therefore, the problem has no single optimal solution but a set of efficient solutions representing the best objective trade-offs. These solutions consist of all design variable vectors for which the corresponding objective vectors cannot be improved in any dimension without disimprovement in another. They are known as Pareto-optimal solutions in reference to the famous economist [1]. Mathematically, Pareto-optimality can be expressed in terms of Pareto dominance. Consider two vectors **X** and **Y** from the design variable space. Then, **X** is said to dominate **Y** if and only if :

$$\begin{aligned} &\forall i = 1..n \qquad f_i(\mathbf{X}) \le f_i(\mathbf{Y}) \\ &\text{and } \exists j \in 1..n \Rightarrow f_j(\mathbf{X}) < f_j(\mathbf{Y}) \end{aligned} \tag{2}$$

All design variable vectors which are not dominated by any other vector of a given set are called *non-dominated* regarding this set. The design variable vectors that are non-dominated over the entire search space are Pareto-optimal solutions and constitute the *Pareto-optimal front*. We illustrate in Fig. 4, the Pareto-dominance of any solution **X** relative to a given solution **Y** in the objective space, for a two dimensional case (n=2).

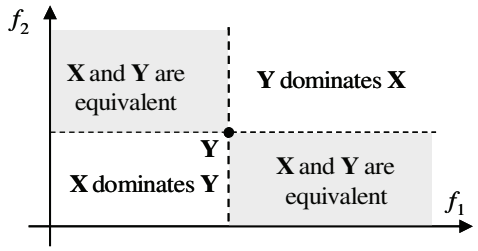

Fig. 4. Pareto-dominance – Two-objective minimization

III.2. Multiobjective Optimization Methods and Decision Making

Multiobjective optimization techniques aim to provide the designer with one or multiple Pareto-optimal solutions. They can be separated into three different classes [2], [3] in relation to the decision making process associated with the optimization procedure. The most popular multiobjective approaches are given in Fig. 5.

- *A priori approaches*: The Decision Maker combines the differing objectives into a global quality function. Thus, the multiobjective problem is transformed into a standard scalar one which can be solved using traditional optimization methods. This approach includes aggregation based methods such as weighting-sum or fuzzy logic techniques, ε–constraint procedure and goal attainment method [2]-[5]. Although they have been widely used in the past, *a priori* techniques have various drawbacks. In particular, in one optimization run, they provide a single Pareto-optimal solution. Moreover, this solution is very sensitive to the objective scalarization and decision parameter choice (e.g. weighting coefficients, target values) associated with the Decision Maker preferences.
- *Progressive and sequential approaches*: The optimization process and the Decision Making are intertwined. The preferences of the Decision Maker are sequentially updated during the optimization process. Note that *a priori* approaches can be iteratively used as progressive approaches as well as traditional techniques such as the lexicographic method. Contrary to many references (e.g. [3]), we choose to classify this method in progressive and sequential approaches because it requires multiple optimization steps to obtain the solution of a given problem
- *A posteriori approaches*: these approaches provide in a single optimization run, a set of Pareto-optimal solutions (Decision Maker can choose among that set). They essentially include population-based optimization methods such as Multiobjective Evolutionary Algorithms (e.g. Genetic Algorithms) [6]-[21] or Multiobjective Particle Swarm Optimization techniques [22]-[24].

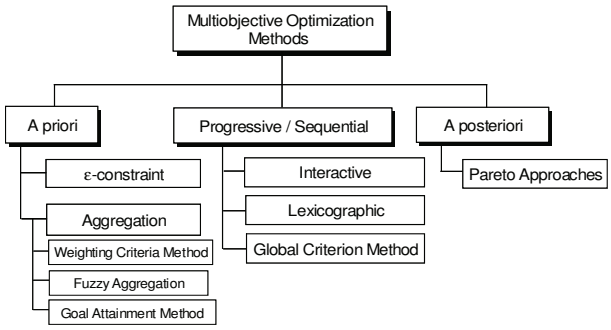

Fig. 5. Classification of multiobjective optimization methods

III.3. Multiobjective Genetic Algorithms

Since the mid-1990s, there has been a growing interest in solving multiobjective problems by Genetic Algorithms. Extensive research in this field has been carried out because of the GA capacity to approximate the set of optimal trade-offs in a single run by investigating multiple solutions in parallel. More than 2000 papers related to this topic are referenced in the EMOO Website [36]. A classification of MOGAs is given in Fig. 6. MOGA approaches can be divided into two groups according to whether they exploit or not the concept of Pareto dominance. Most efficient algorithms

are Elitist MOGAs associated with niching and clustering methods.

Elitist MOGAs use an external population, namely *archive,* which preserves non-dominated individuals in the population. In these algorithms, a fitness assignment procedure is generally used to assess the individual adaptation as a function of their Pareto-dominance. At each generation, individuals (*parents*) selected from the archive (and/or from the population) are crossed and mutated to create new individuals (*children*). The population of children and the archive are merged to assess the non-dominated set of the next generation. If the number of non-dominated individuals is higher than the size of the archive, a *clustering* method is used to preserve most representative solutions and eliminate others in order to keep a constant archive size. Note that a niching procedure [10] is used in the selection process when competing individuals have a similar fitness or a similar Pareto ranking. The skeleton of an Elitist MOGA is given in Fig. 7 and the characteristics of the most popular algorithms of this class are summarized in Table 1.

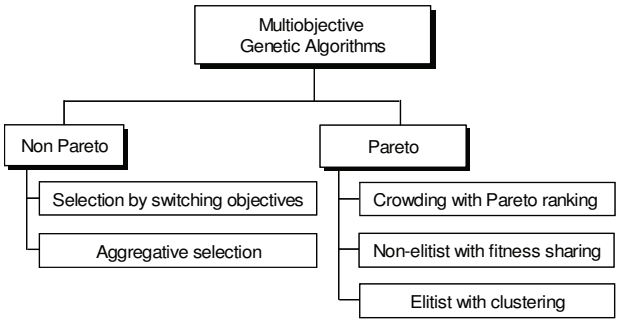

Fig. 6. MOGA classification

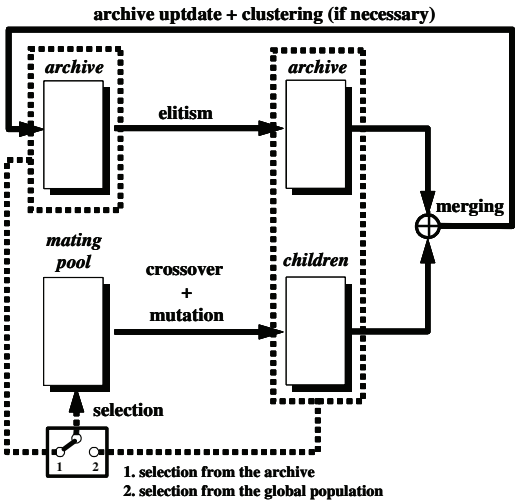

Fig. 7. Structure of an Elitist MOGA (one step generation)

TABLE I
POPULAR ELITIST MOGAS

	Fitness Assignment	Niching Scheme	Clustering
PAES [17] PESA [18]	None Pareto ranking tournaments	Based on a grid in the objective space	Random elimination of non-dominated individuals belonging to the most populated region of the grid
SPEA [16] SPEA2 [19]	Strength	Through fitness assignment	Based on distances between individuals in the population
NSGA-II [20]	None Pareto ranking tournaments	Density estimation (*I*-distance)	Based on *I*-distance

III.4. Description of the NSGA-II

We specifically present the second version of the Non-dominated Sorting Genetic Algorithm (NSGA-II) which has been used to show the interest of MOGAs in the IOD context. NSGA-II is based on the principles previously given. It determines all successive fronts in the population (the best front corresponding to the non-dominated set). Moreover, a *crowding distance* called *I-distance* estimates the density of solutions surrounding each individual on a given front. The computation of the *I*-distance is given by the following pseudocode [20] :

For each individual belonging to a front F of size $l = |F|$
Set $I(i)_{distance} = 0$
For each objective n
  Sort individual of the front F using the nth objective value
  Set $I(1)_{distance} = I(l-1)_{distance} = \infty$
  For i = 2 to l-1

$$I(i)_{distance} = I(i)_{distance} + \frac{f_n(i+1) - f_n(i-1)}{f_n(l) - f_n(1)}$$

where $f_n(i)$ denotes the n-th objective relative to the i-th individual of the front F. Note that contrary to [20], implicit scalarization of the objectives is carried out by normalizing the *I-distance* with the maximum objective deviation. An example of *I-distance* computation is illustrated in Fig. 8 for a two objective problem.

The *I*-distance density estimator index is then used in the selection and the clustering procedures:

- in a tournament, if individuals belong to the same front, the selected one has the greater *I*-distance.

- at the end of a generation, individuals of the global population (created children and archive elements of the current generation) are sorted in relation to their Pareto rank (i.e. the front they belong to, the first front being composed of non-dominated individuals). Then individuals of each front are resorted according their *I*-distance by giving preference to individuals of greater *I*-distance (extreme solutions of the front and isolated

individuals). Finally, the new archive is obtained by truncation from this widened population considering the previous sorts. It should be noted that one particularity of the NSGA-II resides in the fact that the archive is diversified since it can contain non-dominated individuals as well as individuals of the successive dominated fronts. Finally, we implement the NSGA-II with the self-adaptive recombination scheme described in [21] to increase its robustness.

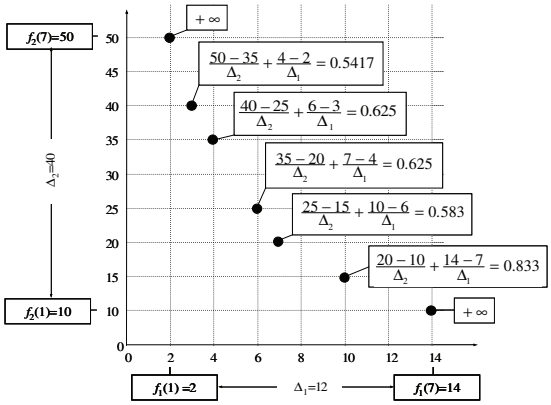

Fig. 8. Example of *I*-distance computations

III.5. Design constraint handling in MOGAs

Some specificities of the IOD approach require the adaptation of standard MOGAs to take all design constraints into account. Contrary to mathematical problems, constraints cannot be simultaneously evaluated but have to be sequentially computed. For instance, it is obvious that it is not possible to determine constraints and objectives related to a given system if one of its elements is itself non-feasible. Consequently, for each IOD problem, a *constraint graph* can be established characterizing the couplings and the sequence of the design constraints in the system model. A constraint graph example is given in Fig. 9 as an illustration. Note that the constraint graph can be decomposed into different levels to facilitate its analysis. Only constraints belonging to the same level can be computed in parallel. Note that objectives are also subject to this representation and can figure in the constraint graph.

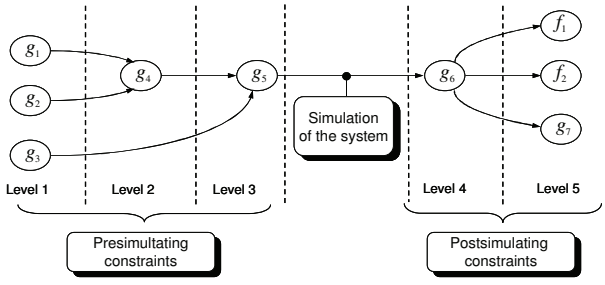

Fig. 9. Illustration of the constraint graph concept

In the example of Fig. 9, it can be seen that the objectives are computable if the constraints g_1 to g_6 are fulfilled, the last constraint being assessable in parallel. The higher the number of levels in the graph, the more difficult the problem. Furthermore, in IOD problems, constraints can be divided into two groups according to whether their determination is done before or after the system simulation (main cost in CPU time). On the one hand, *presimulating* constraints are mainly "local" relative to specific elements of the system or to their association in the system. On the other hand, *postsimulating* constraints are essentially "global" concerning the whole system. As underlined before, the sequential computation of the constraint increases the difficulty of the optimization problem. Violated constraints act as a barrier with regard to the optimization algorithm which is in addition "blind" towards non-computable constraints of the higher levels. In practice, when a constraint $g(\mathbf{X})$ cannot be computable (because it depends on another violated constraint at a lower level in the graph) we chose to assign for its value the maximum penalty (death penalty) i.e. $g(\mathbf{X}) = +\infty$. To take into account the design constraints in MOGAs, the Pareto-dominance rule can be modified as follows:

- if two individuals are non-feasible, the Pareto-dominance relative to these individuals is applied in the constraint space.
- if two individuals are feasible, the Pareto-dominance relative to these individuals is applied in the objective space.
- if one individual is feasible and the other non-feasible, the feasible individual dominates the non-feasible individual.

In this manner, Pareto ranking tournaments between individuals include the constraint minimization as well as the objective minimization. Note in the case of the NSGA-II, for non-feasible individuals belonging to a given front in the constraint space, the computation of the *I-distance* density estimator is carried out in relation to all constraints. In this way, niching will occur in the two different spaces (i.e. constraint and objective space) and diversity will be preserved to avoid premature convergence.

IV. The PEV Design Model

There is an important volume of research carried out in the field of electric vehicles. Most advanced solutions from the technical and economic point of view are hybrid structures which combine an internal combustion engine with an electrical motor associated with storage elements (batteries or supercapacitors). PEVs suffer from problem related to the embedded energy storage. In effect, the ratio Energy/Mass is significantly lower for standard electrochemical accumulators in comparison

with those of petroleum fuels. Therefore, even if PEVs are theoretically energetically more efficient than standard fuel vehicles (FVs), they are strongly penalized by a higher mass. Improvement of PEVs in relation to FVs implies the reduction of the mass disadvantage of electrochemical accumulators. On the other hand, some innovative and interesting solutions can emerge by using an IOD approach. As a case study, we investigate the IOD of traction devices for PEVs. The considered system corresponds to the example of Fig. 2. It is composed of a lithium-ion battery, a power DC-AC converter and a permanent magnet synchronous electrical motor associated with a reducer of fixed ratio. In the next subsections, we specify some particularities concerning the different models and technological data with regard to the parameterization of the system.

IV.1. The Electrochemical Lithium-ion Accumulator Model

The battery is made up of elementary cells associated in series and in parallel, the total number of cells being obtained by multiplying the number of cells in series (n_s) with the number of branch (n_p) in parallel. Each cell can be represented by an internal resistance R_0 in series with an internal voltage E_0. This electromotive force depends on the state of charge *SOC* of the cell which evolves during the driving cycle of the vehicle following Peukert's law [26]. For technological reasons, the electromotive force is bounded by two values determined by the manufacturer ($E_0^{\min} \le E_0 \le E_0^{\max}$). The *SOC* variations (ΔSOC) are related to the current I_{cell} provided (or absorbed during the braking phases) by the cell and to the charge capacity C_3 (defined for a discharge in 3 hours at constant current $I_3 = C_3/3$).

$$\Delta SOC_k = \frac{I_{\text{cel}_k}}{C_i}\Delta t_k = \frac{I_{\text{cell}_k}}{C_3}\left(\frac{I_{\text{cel}_k}}{I_3}\right)^{n-1}\Delta t_k \qquad (3)$$

where k denotes the time step index, Δt_k the corresponding time variation, and n is the Peukert coefficient (typically n = 1.1 for lithium-ion cells). Note that the accumulator cell state of charge is maximum at the beginning of the driving cycle (*SOC* = 1 and $E_0 = E_0^{\max}$). Three different kinds of lithium-ion cells of the SAFT manufacturer [35], whose characteristics are given in Table II, are considered in the IOD process. "Partial" objectives related to the battery are computed from these data. Accumulator losses P_{bat} are represented by Joule losses in the internal resistance of each cell. They are deduced from the R_0 value and from the I_{cell} current obtained during the driving cycle. The battery mass is evaluated from the mass of one cell and from the total number of cells ($n_{cell} = n_p \times n_s$).

TABLE II
CHARACTERISTICS OF THE ACCUMULATOR CELLS IN THE IOD PROCESS

Cell Type	C_3 Capacity	Internal Resistance R_0	Mass	Internal Voltage $E_0^{\min}$	Internal Voltage $E_0^{\max}$
1	39 A.h	7 mΩ	1.05 kg	2.7 V	4 V
2	25 A.h	16.75 mΩ	0.75 kg	2.7 V	4 V
3	16 A.h	23 mΩ	0.68 kg	2.7 V	4 V

IV.2. The DC-AC Converter Model

The electric motor control is ensured with a DC-AC converter operating at the F_{switch} switching frequency. The voltage inverter is composed of six IGBT power semiconductors in association with antiparallel diodes to guarantee current reversibility. Inverter losses P_{inv} are computed by means of an analytical model which takes into account switching losses P_{switch} and conduction losses P_{cond} [27]

$$\begin{aligned} P_{switch} &= 6\frac{F_{switch}}{2\pi}\int_{\varphi}^{\varphi+\pi}\left[W_{on}(\theta)+W_{off}(\theta)\right]\mathrm{d}\theta \\ &= 6F_{switch}\left(\frac{a_{on}+a_{off}}{2}+\left(b_{on}+b_{off}\right)\frac{I_{\max}}{\pi}\right. \\ &\qquad \left.+\left(c_{on}+c_{off}\right)\frac{I_{\max}^2}{4}\right) \end{aligned} \qquad (4)$$

$$\text{with} \quad \begin{cases} W_{on} = a_{on} + b_{on}I_c + c_{on}I_c^2 \\ W_{off} = a_{off} + b_{off}I_c + c_{off}I_c^2 \end{cases} \qquad (5)$$

where I_{max} denotes the maximum value of the motor current and a_{on}, b_{on}, c_{on} (respectively a_{off}, b_{off}, c_{off}) are interpolating coefficients obtained from the turn-on (respectively the turn-off) energy curve given by the manufacturer data sheets. Conduction losses depend on the modulation factor m_a, on the maximum motor current I_{max} and on the technological characteristics of the diodes ($V_{D(on)}$, $R_{D(on)}$) and IGBTs ($V_{CE(on)}$, $R_{IGBT(on)}$) :

$$\begin{aligned} P_{cond} &= 6\left(V_{D(on)}\,I_{mean} + R_{D(on)}\,I_{D\_rms}^2\right) \\ &\quad + 6\left(V_{CE(on)}\,I_{mean} + R_{IGBT(on)}\,I_{IGBT\_rms}^2\right) \end{aligned} \qquad (6)$$

$$\text{with} \quad \begin{cases} I_{mean} = \dfrac{I_{\max}}{2\pi}\left(1+\dfrac{\pi}{4}m_a\cos\varphi\right) \\ I_{D\_rms}^2 = \dfrac{I_{\max}^{\,2}}{8}\left(1-\dfrac{8}{3\pi}m_a\cos\varphi\right) \\ I_{IGBT\_rms}^2 = \dfrac{I_{\max}^{\,2}}{8}\left(1+\dfrac{8}{3\pi}m_a\cos\varphi\right) \end{cases} \qquad (7)$$

$$\text{and} \quad m_a = 2\sqrt{2}V_m/V_{bat} \qquad (8)$$

where φ represents the phase between the motor current I_m and the motor voltage V_m and where V_{bat} is the battery voltage.

A thermal model of the inverter based on classical

state-circuit representation allows us to deduce the temperature on the IGBT-diode pack module and the thermal resistance of the radiator R_{TH_RAD}, to operate at the specified temperature conditions (in particular, the module temperature must not exceed 100°C). This model is represented in Fig. 10. Finally, the radiator mass M_{rad}, which approximates the inverter mass, is deduced from its length l_{rad} and the mass density per unit length (typically 14.58 kg for a AAVID THERMALLOY OSX43 [37]). For this radiator, the length l_{rad} can be obtained from the thermal resistance R_{TH_RAD} by interpolating manufacturer data (see Fig. 11).

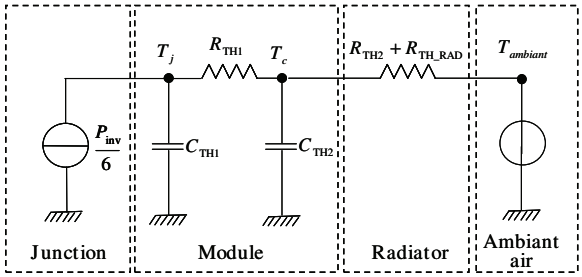

Fig. 10. The inverter thermal model

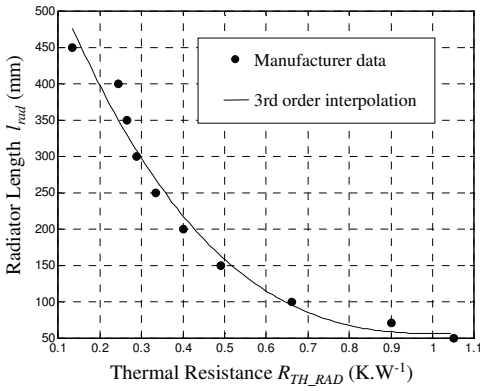

Fig. 11. The Radiator Sizing

TABLE III
CHARACTERISTICS OF THE INVERTER POWER MODULES IN THE IOD PROCESS

	MII200-12A4	MII300-12A4	MII400-12E4
I_{c25}	270	330	420
$R_{IGBT(on)}$	7 mΩ	6.2 mΩ	5.3 mΩ
$V_{CE(on)}$	1.5 V	1.3 V	1.0 V
$R_{D(on)}$	3.4 mΩ	2.4 mΩ	1.3 mΩ
$V_{D(on)}$	1.3 V	1.3 V	1.3 V
a_{on}	0.075	0.01	0.002
b_{on}	0.0	3.25e-5	-8.33e-6
c_{on}	6.66e-7	3.97e-7	3.83e-7
a_{off}	0.005	0	0
b_{off}	1.33e-4	1.65e-4	1.083e-4
c_{off}	0	-7.5e-8	-2.77e-8
V_{max}	1200 V	1200 V	1200 V
R_{TH1}	0.11 K/W	0.088 K/W	0.078 K/W
R_{TH2}	0.003 K/W	0.002 K/W	0.002 K/W
C_{TH1}	0.4 J/K	0.5 J/K	0.52 J/K
C_{TH2}	0.93 J/K	1.16 J/K	1.29 J/K

Three kinds of IGBT modules of the IXYS manufacturer [36] (referenced MII200-12A4, MII300-12A4, and MII400-12E4) are considered in the IOD process. The characteristics of these modules are given in Table 3.

IV.3. The Synchronous Motor Model

The sizing model of the Permanent Magnet Synchronous Motor (PMSM) is developed in [27], [28]. It depends on geometrical characteristics (number p of pole pairs, number N_{spp} of slots per pole per phase, radius / length ratio $R_{rl} = r_s/l_r$) as well as electro-mechanical features (current density J_s, base speed Ω_b and corresponding base torque T_b).

- *The Geometric Model*

The geometrical characteristics of the motor are illustrated in Fig. 12. The bore radius r_s is related to the fundamental value of the air gap magnetic flux density (B_{1g}) and to the slot depth / bore radius ratio R_{dr} as follows:

$$r_s = \left(T_b R_{rl} \frac{1}{J_s K_r B_{1g} R_{dr} \pi} \right)^{\frac{1}{4}} \tag{9}$$

where K_r is the slot filling coefficient. B_{1g} is computed from the magnet properties (relative permeability $\mu_r = 1.05$ and remanent induction $B_r = 1.1$ T for NdFeB magnet) and from the electrical half pole width α_m:

$$B_{1g} = \frac{4}{\pi} B_r \frac{l_m / g'}{\mu_r + (l_m / g')} \sin(\alpha_m) \tag{10}$$

where l_m/g' represents the ratio between the magnet thickness and the air gap corrected by the carter coefficient.

In these two equations, the unknown variables are set to typical values, i.e. $R_{dr} = 0.25$, $K_r = 0.5$, $\alpha_m \approx 1.31$ (i.e. 75°) and $l_m/g' = 3.5$ and the Carter coefficient is neglected ($K_c \approx 1$ which implies $g'=g$).

The magnet width w_m can be deduced as follows:

$$w_m = \frac{r_s \alpha_m}{p} \tag{11}$$

The motor air gap g is calculated from the empiric relation:

$$g = 0.001 + 0.003 r_s / \sqrt{R_{rl}} \tag{12}$$

Tooth and slot widths are then obtained from the bore radius and the number of slots per pole per phase N_{spp}:

$$w_S = w_T = \frac{\pi\, r_s}{6pN_{spp}} \tag{13}$$

and the slot depth d_S is given by:

$$d_S = R_{dr} r_s \tag{14}$$

Finally, the yoke thickness is obtained as follows:

$$d_y = \frac{r_s}{p}\alpha_m \frac{\hat{B}_g}{\hat{B}_y} \tag{15}$$

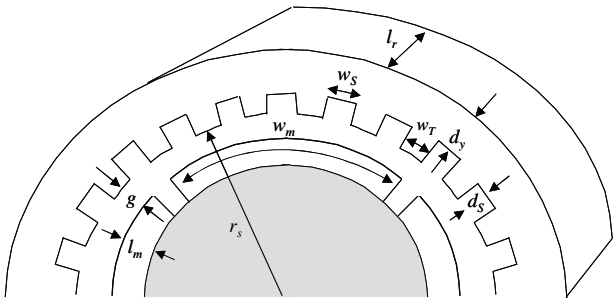

Fig. 12. The geometrical characteristics of the PMSM

where the yoke induction is set to 1.6 T and where the maximum magnetic flux density in the air gap is evaluated from the following relation:

$$\hat{B}_g = B_r \frac{l_m / g'}{\mu_r + l_m / g'} \tag{16}$$

- *The Circuit Model*

Electric circuit parameters of the motor are computed from the previous geometric variables. In particular, leakage inductances L_l are obtained from [34] by considering a trapezoidal slot as shown in Fig. 13.

$$L_l = 2\mu_0 l_r pN_{spp}\lambda_s N_{cs}^2 \tag{17}$$

where N_{cs} denotes the number of conductors per slot and where the λ_s coefficient depends on the slot geometrical characteristics (18), (19).

$$\lambda_s = \frac{2h_1}{3(b_1 + b_3)} + \frac{2h_2}{b_2 + b_3} + \frac{h_3}{b_2} \tag{18}$$

with

$$\begin{cases} h_1 = 8d_S K_r / 7 \\ h_2 = w_S / 8 \\ h_3 = 0.02 r_s \\ b_1 = w_S \\ b_2 = w_S / 2 \\ b_3 = 3w_S / 4 \end{cases} \tag{19}$$

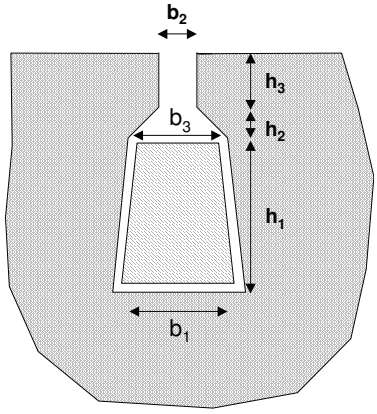

Fig. 13. The geometrical characteristics of a slot

The main inductance L_p, the magnetic flux Φ_s and the stator resistance R_s can be also expressed as a function of N_{cs}:

$$L_p = \frac{6\mu_0 r_s l_r}{\pi(K_c g + l_m)} N_{spp}^2 K_{1b}^2 N_{cs}^2 \tag{20}$$

$$\Phi_s = 2K_{1b} N_{spp} B_{1g} r_s l_s N_{cs} \tag{21}$$

$$R_s = 12\rho_{copper}\left[l_r + \frac{\pi^2(r_s + 0.5d_S)}{2p}\right]\frac{p^2 N_{spp}}{\pi\, r_s d_S K_r} N_{cs}^2 \tag{22}$$

where the winding factor K_{1b} is approximated with:

$$K_{1b} = \frac{\sin\frac{\pi}{6}}{N_{spp}\sin\frac{\pi}{6N_{spp}}} \tag{23}$$

Note also that the motor current I_m can be obtained from the current density J_s as follows:

$$I_m = \frac{J_s d_s K_r \pi\, r_s}{6pN_{spp}N_{cs}} \tag{24}$$

To compute all circuit parameters of the motor, the number of conductors N_{cs} in one slot has to be determined. It should be designed in order to fulfill operating conditions at the base point. The permanent magnet machine must be able to provide the base torque $T_m = T_b$ under supply voltage $V_m = V_b$ at the electrical pulsation $\omega = \omega_b$. By setting $N_{cs} = 1$ in (17), (20), (21), (22) and (24) circuit variables L_{l1}, L_{p1}, Φ_{s1} R_{s1} and I_{m1} can be obtained from one conductor per slot, which implies:

$$\begin{cases} L_l = N_{cs}^2 L_{l1} \\ R_s = N_{cs}^2 R_{s1} \\ L_p = N_{cs}^2 L_{p1} \\ \Phi_s = N_{cs} \Phi_{s1} \\ I_m = I_{m1} / N_{cs} \end{cases} \quad (25)$$

By considering the electrical diagram of the motor (see Fig. 14), operating at the base point (T_b, ω_b), the number of conductors in one slot can be deduced as:

$$N_{cs} = \frac{V_b}{\sqrt{(\Phi_{s1}\omega_b + R_{s1} I_{m1})^2 + ((\frac{3}{2} L_{p1} + L_{l1})\, I_{m1}\omega_b)^2}} \quad (26)$$

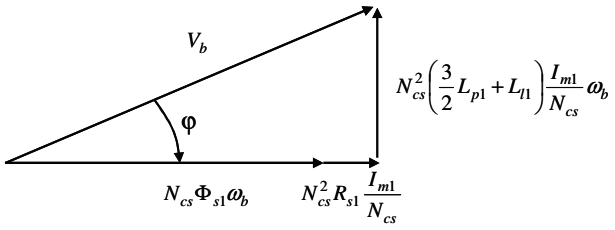

Fig. 14. The electrical diagram of the motor at the base point

Geometric and electric parameters are thus completely known. Indeed, the motor behavior can be characterized in transient mode using a standard model based on Park's equations. The control law allows reaching torque and speed specifications required by the driving cycle. According to the system working point, the motor is controlled with a strategy operating in maximum torque per ampere capacity or in defluxing mode.

- *The Thermal Model*

An additional circuit model simulates the thermal behavior of the motor in each of these constitutive elements (slot copper, slot insulation, stator yoke) in relation to their thermal characteristics (thermal resistance and capacity of the corresponding elements) and external conditions (i.e. the surrounding temperature). This model is coupled to electromagnetic phenomena through iron and Joule losses (see Fig. 15).

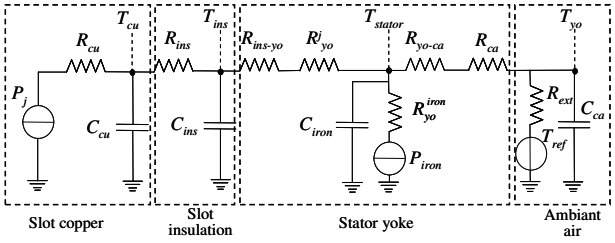

Fig. 15. The thermal model of the motor

The thermal resistances of this model are given by the following equations:

$$R_{cu} = \frac{1}{4\pi l_r \lambda_{cu}} \left[1 - 2 \left(\frac{R_1^2}{R_2^2 - R_1^2} \right) \ln \frac{R_2}{R_1} \right] \quad (27)$$

$$R_{ins} = \frac{\ln \frac{R_3}{R_2}}{2\pi \lambda_{ins} l_r} \quad (28)$$

$$R_{ins-yo} = \frac{1/300}{2\pi l_r R_3} \quad (29)$$

$$R_{yo}^j = \frac{\ln \frac{R_5}{R_4}}{2\pi \lambda_{yo} l_r} \quad (30)$$

$$R_{yo}^f = \frac{1}{4\pi l_r \lambda_{yo}} \left[1 - 2 \left(\frac{R_4^2}{R_5^2 - R_4^2} \right) \ln \frac{R_5}{R_4} \right] \quad (31)$$

$$R_{yo-ca} = \frac{1/1500}{2\pi l_r R_5} \quad (32)$$

$$R_{ca} = \frac{\ln \frac{R_7}{R_6}}{2\pi \lambda_{ca} l_r} \quad (33)$$

$$R_{ca} = \frac{\ln \frac{R_7}{R_6}}{2\pi \lambda_{ca} l_r} \quad (34)$$

$$R_{ext} = \frac{1}{h(2\pi R_7 l_r + 2\pi R_7^2)} \quad (35)$$

where the geometric variables R_1, R_2, R_3, R_4, R_5, R_6 and R_7 are defined as follows:

$$\begin{cases} R_1 = r_s \\ R_2 = r_s + d_S \\ R_3 = R_2 + 0.003 \\ R_4 = R_3 \\ R_5 = R_4 + d_y \\ R_6 = R_5 \\ R_7 = R_6 + 0.01 \end{cases} \quad (36)$$

Note that in these equations, thermal conductivities of the materials (copper, insulator, iron and aluminum) are set to typical values, i.e. λ_{cu}=5 W.m^{-1}.K^{-1}, λ_{ins}=0.25 W.m^{-1}.K^{-1}, λ_{yo}=25 W.m^{-1}.K^{-1}, and λ_{ca}=180 W.m^{-1}.K^{-1}.

The thermal capacities associated in the circuit model are calculated as follows:

$$C_{cu} = \frac{\pi l_r K_r [(r_s + d_S)^2 - r_s^2] \rho_{cu} C_{pcu}}{12 p N_{spp}} \quad (37)$$

$$C_{ins} = \frac{\pi \left(R_3^2 - R_2^2 \right) \rho_{ins} C_{pins}}{6 p N_{spp}} \quad (38)$$

$$C_{iron} = \frac{1}{6pN_{spp}}\left(\pi l_r\left[(r_s + d_S + d_y)^2 - (r_s + d_S)^2\right] + \frac{1}{2}\pi l_r\left[(r_s + d_S)^2 - r_s^2\right]\right)\rho_{iron}C_{piron} \quad (39)$$

$$C_{ca} = \frac{\pi l_r\left(R_7^2 - R_6^2\right)\rho_{alu}C_{alu}}{6pN_{spp}} \quad (40)$$

where the mass density per volume and the thermal capacity of the materials are:

$$\begin{cases} \rho_{cu} = 8953\ \text{kg.m}^{-3} & C_{pcu} = 398\ \text{J.kg}^{-1}\text{K}^{-1} \\ \rho_{ins} = 1200\ \text{kg.m}^{-3} & C_{pins} = 1250\ \text{J.kg}^{-1}\text{K}^{-1} \\ \rho_{iron} = 7650\ \text{kg.m}^{-3} & C_{piron} = 460\ \text{J.kg}^{-1}\text{K}^{-1} \\ \rho_{al} = 2787\ \text{kg.m}^{-3} & C_{pal} = 883\ \text{J.kg}^{-1}\text{K}^{-1} \end{cases}$$

- *The calculation of motor masses*

The motor masses are obtained from the volume of each constitutive element and the corresponding mass density. The rotor volume V_{rotor} can be approximated by:

$$V_{rotor} = \pi l_r(r_{rotor}^2 - (r_{rotor} - d_R)^2) \quad (41)$$

where $r_{rotor} = r_s - g - l_m$ and $d_R = d_y$. The corresponding mass is given by:

$$M_{rotor} = V_{rotor}\rho_{iron} \quad (42)$$

The stator volume V_{stator} is composed of yoke and teeth volumes

$$V_{stator} = V_{teeth} + V_{yoke} \quad (43)$$

which can be approximated as follows:

$$\begin{cases} V_{yoke} = 2\pi l_r d_y\ (r_s + d_S + d_y/2) \\ V_{teeth} = \pi l_r d_S\ (r_s + d_S/2) \end{cases} \quad (44)$$

The corresponding mass is

$$M_{stator} = V_{stator}\rho_{iron} \quad (45)$$

Total iron mass in the motor can be expressed by summing stator and rotor iron masses

$$M_{iron} = M_{stator} + M_{rotor} \quad (46)$$

Similarly, the magnet volume is given by:

$$V_{magnet} = \pi l_r K_p\left((r_s - g)^2 - r_{rotor}{}^2\right) \quad (47)$$

and the corresponding mass by:

$$M_{magnet} = \rho_{magnet}V_{magnet} \quad (48)$$

with $\rho_{magnet} = 7400$ kg.m^{-3}. Finally, the copper mass is deduced from the copper volumes in the slots and in the winding heads

$$\begin{cases} V_{copper}^{slot} = \pi l_r K_r d_S(r_S + d_S/2) \\ V_{copper}^{head} = 3\pi^3(r_s + d_S/2)d_S w_S K_r N_{spp} \end{cases} \quad (49)$$

which implies

$$M_{copper} = \rho_{copper}(V_{copper}^{head} + V_{copper}^{slot}) \quad (50)$$

The total mass of the motor is then approximated by summing the masses related to each component:

$$M_{motor} = M_{iron} + M_{copper} + M_{magnet} \quad (51)$$

- *The calculation of motor losses*

Iron losses in the motor are divided into hysteresis (P_{Hyst}) and eddy current losses (P_{Eddy}) in the stator parts (i.e. yoke and teethes). Iron losses in the yoke are computed as follows [29] :

$$\begin{cases} P_{Hyst}^{yoke} = V_{yoke}\dfrac{2K_H}{\pi}\hat{B}_y{}^2\omega \\ P_{Eddy}^{yoke} = V_{yoke}\dfrac{8\alpha_p}{\pi K_p}\hat{B}_y{}^2\omega^2 \end{cases} \quad (52)$$

where the filling coefficient K_p equals 0.833 and where K_H and α_p are empiric factors depending on the material (typically K_H = 52 and α_p = 0.06 for FeSi 3%). Similarly, iron losses in the teethes can be deduced by the following relation

$$\begin{cases} P_{Hyst}^{teeth} = V_{teeth}\dfrac{2K_H}{\pi}\hat{B}_{teeth}{}^2\omega \\ P_{Eddy}^{teeth} = V_{teeth}\dfrac{24\alpha_p N_{spp}}{\pi}\hat{B}_{teeth}{}^2\omega^2 \end{cases} \quad (53)$$

with

$$\hat{B}_{teeth} = \frac{\hat{B}_g}{0.5 + \dfrac{d_S}{3r_s}} \quad (54)$$

Global iron losses in the motor are then obtained by summing all hysteresis and eddy current losses:

$$P_{iron} = P_{Hyst}^{yoke} + P_{Eddy}^{yoke} + P_{Hyst}^{teeth} + P_{Eddy}^{teeth} \quad (55)$$

Joule losses P_j are also added to compute total motor losses:

$$P_j = 3R_s I_m^2 \tag{56}$$

Note that copper losses have been neglected in this model.

IV.4. The Reducer Model

The mechanical transmission line of the vehicle from the motor to the wheels is assimilated to a reducer of fixed ratio. A simplified analytical model [30] allows us to assess the reducer sizing variables from the dimensioning torque T_{red}, the reducer ratio N, and the corresponding partial objectives (i.e. the reducer loss P_{red} and M_{red} mass). The structure of the reducer is illustrated in Fig. 16.

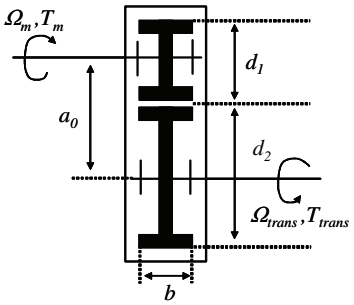

Fig. 16. The reducer model

The sizing variables of the reducer are defined by the empiric relations:

$$d_1 = \sqrt[3]{\frac{4.2T_{red}}{12.8\times10^6 \dfrac{N}{N+1}}} \tag{57}$$

$$d_2 = Nd_1 \tag{58}$$

$$b = 0.8d_1 \tag{59}$$

The mass of the reducer is approximated by:

$$M_{\text{red}} = K_{\text{red}}\rho_{\text{red}}\, b\, \left((0.5d_1)^2\pi + (0.5d_2)^2\pi\right) \tag{60}$$

where ρ_{red} = 7650 kg.m^{-3} and K_{red} = 1.1.

The reducer efficiency η_{red} is assumed to be linear, varying from 1 to 0.9 for reducer ratios between 1 and 10. Reducer losses are computed as follows:

$$P_{red} = \left(\frac{1-\eta_{red}}{\eta_{red}}\right) T_{trans}\Omega_{trans} \tag{61}$$

IV.5. The Dynamic Model of the PEV

To simulate the vehicle's course, the torque and the speed imposed on the electrical motor must be known. These variables depend on the driving cycle of the vehicle i.e. on particular speed profiles and specific road profiles (typically a road slope during the course) as well as external conditions (wind velocity, road-wheel grip). A mechanical model [31] simulates the efforts imposed on the vehicle (i.e. vehicle weight, drag force, acceleration force) and provides torque and speed references for the electrical traction motor.

The global effort F_{tot}, imposed to the vehicle on its course, can be decomposed as follows:

$$F_{tot} = F_{roll} + F_{aero} + F_{grav} + F_{acc} \tag{62}$$

The rolling resistance F_{roll} force is defined as:

$$F_{roll} = f_r Mg \tag{63}$$

where g denotes the acceleration of gravity, M represents the total mass of the vehicle (including a frame mass of 800 kg) and f_r is the rolling resistance coefficient. For radial tires, this coefficient is approximated as a function of the vehicle speed V, by the empiric relation

$$f_r = 0.0051 + 0.000051V \tag{64}$$

By neglecting the wind velocity, the aerodynamic drag force F_{aero} essentially depends on the vehicle speed, on the drag coefficient C_x and on the vehicle section area S

$$F_{aero} = \frac{1}{2}\rho_{air} S C_x V^2 \tag{65}$$

where the density of air ρ_{red} is set to 1.293 kg.m^{-3}. Note that we use typical values for C_x and S (S = 2 m^2 and C_x = 0.4)

The force due to the gravity F_{grav} is expressed according to the road slope θ:

$$F_{grav} = Mg\sin\theta \tag{66}$$

and the acceleration force F_{acc} is classically defined as:

$$F_{acc} = M\frac{dV}{dt} \tag{67}$$

Finally, torque and speed on the mechanical transmission can be deduced from the global effort on the vehicle and the corresponding velocity

$$\begin{cases} T_{trans} = F_{tot} r \\ \Omega_{trans} = V / r \end{cases} \tag{68}$$

where r denotes the wheel radius (typically r = 0.33 m)

IV.6. The Driving Cycle

Some driving cycles established by the INRETS (the French national institute for transport and safety research) corresponds to typical cycles obtained from statistical studies on real vehicle courses [32]. Road profiles can be considered flat (i.e. θ=0) without loss of generality. Two different specific cycles are investigated:

- The *urban driving cycle* described by Fig. 17 and characterized by low speeds (40 km/h on average) with a maximum peak value at 90 km/h. The cycle duration is 1374 s (i.e. about 23 min) and the corresponding course with regard to the considered speeds equals 12.2 km. Note that this elementary cycle has to be repeated 16 times to achieve a minimum range of 200 km for the vehicle.

- The *road driving cycle* described by Fig. 18 which presents higher speed values with a maximum peak at 120 km/h. The cycle duration is 734 s (i.e. about 12 min) and the corresponding course with regard to the considered speeds equals 15.4 km. In this case, the elementary cycle has to be repeated 13 times to achieve a minimum range of 200 km for the vehicle.

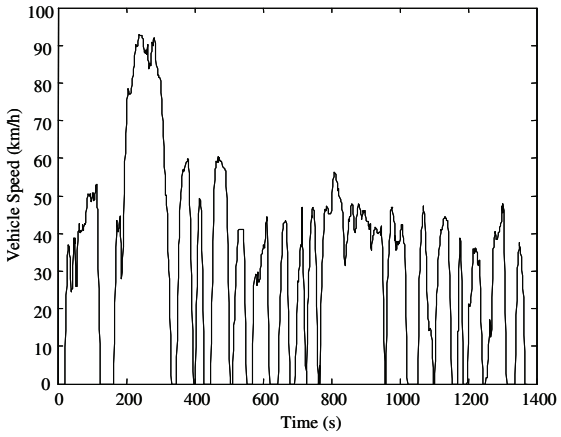

Fig. 17. The urban driving cycle

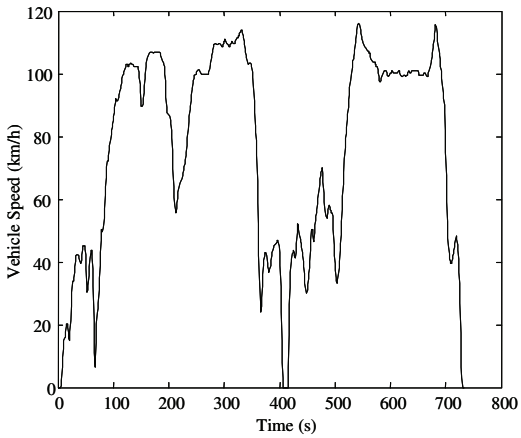

Fig. 18. The road driving cycle

V. IOD Example: Optimization of Traction Devices for Pure Electric Vehicles

In this section, we illustrate the application of MOGA's to the IOD of PEVs with the aim at minimizing the total losses and the embedded mass (i.e. the mass of the traction device) in the vehicles.

V.1. The Design Variables

All design variables and their corresponding bounds considered in the IOD process, are given in Table IV. Seven variables associated with the sizing and energetic parameters are continuous whereas six variables related to the system structure are discrete.

TABLE IV
DESIGN VARIABLE CHARACTERISTICS

Design Variable	Nature	Bounds
Battery		
Number of cells in series	Discrete	$n_s \in \{1,..,200\}$
Cell branches in parallel	Discrete	$n_p \in \{1,..,200\}$
Type of cells	Discrete	$Cell \in \{1, 2, 3\}$
Inverter		
Switching Frequency	Continuous	$F_{switch} \in [0.001, 100]$ [kHz]
IGBT Type	Discrete	$IGBT \in \{1, 2, 3\}$
Permanent Magnet Synchronous Motor		
Radius/length ratio	Continuous	$R_{rl} \in [0.1, 10]$
Number of pole pairs	Discrete	$p \in \{1,..,10\}$
Number of slots/pole/phase	Discrete	$N_{spp} \in \{1, 2, 3\}$
Current density	Continuous	$J_s \in [1, 10]$ [A/mm^2]
Base torque	Continuous	$T_b \in [1, 2000]$ [N.m]
Base speed	Continuous	$\Omega_b \in [1, 10\,000]$ [rad/s]
Mechanical Reducer		
Reducer ratio	Continuous	$N \in [1, 10]$
Sizing torque	Continuous	$T_{red} \in [1, 2000]$ [N.m]

V.2. The Design Constraints

Twelve constraints must be fulfilled to ensure the PEV feasibility and to allow it to comply with the driving cycle. In particular, the constraint graph resulting from the sizing and simulating models can be obtained and divided into three levels:

- the first level is constituted by two constraints (g_1 and g_2) associated with the electrical motor sizing. They concern the number of copper windings per slot. This number has to be higher than one and bounded by the slot section in relation to the minimum winding section $S_{winding}$ (this last is set to 0.5 mm²).

$$g_1 = 1 - N_{cs} \le 0 \tag{69}$$

$$g_2 = S_{winding} - \frac{d_S w_S K_r}{N_{cs}} \le 0 \tag{70}$$

- the constraints of the next level ensure that the electrical motor is capable of operating at its base point (T_b, Ω_b) in permanent operating mode. In particular, a specific constraint (g_3) related to the maximum stator flux density (itself coupled with the motor current) and the magnet flux density prevents magnet demagnetization

$$g_3 = \hat{B}_S(T_b, \Omega_b) - \hat{B}_g - B_D \leq 0 \quad (71)$$

with B_D is set to −0.2 T and where

$$\hat{B}_S(T_b, \Omega_b) = \frac{J_s d_S w_S K_{1b} K_r \sqrt{2} r_s \mu_0}{p(w_S + w_T)(K_c g + \frac{l_m}{\mu_r})} \quad (72)$$

An additional constraint (g_4) verifies that the temperature of the copper windings does not exceed the critical limit of insulators (i.e. 160°C):

$$g_4 = T_{copper}(T_b, \Omega_b) - 160° \leq 0 \quad (73)$$

- the constraints of the third level are related to the fulfillment of the driving cycle. Firstly, three specific constraints are associated with the electrical motor. As previously for the base point, the motor magnet demagnetization and the thermal constraint on copper windings have to be assessed in transient operating mode during the vehicle course. Therefore, two additional constraints g_5 and g_6 (respectively similar to g_3 and g_4) are computed for each point (T_m, Ω_m) of the driving cycle.

$$g_8 = \sum_k \max(0,\ B_S^k(T_m, \Omega_m) - \hat{B}_g - B_D) \leq 0 \quad (74)$$

$$g_6 = \sum_k \max(0,\ T_{copper}^k(T_m, \Omega_m) - 140°) \leq 0 \quad (75)$$

An additional constraint g specifies that all cycle points are reachable in standard or defluxing mode

$$g_7 = \sum_k R_k(T_m, \Omega_m) \leq 0 \quad (76)$$

where k represents a cycle point and with $R_k(T_m, \Omega_m) = 0$ if the k^{th} cycle point is reachable and $R_k(T_m, \Omega_m) = 1$ if not. The next constraints concern the DC-AC converter. In particular, the temperature on the semiconductor junctions does not exceed 125°C. Therefore, the g_8 constraint must be fulfilled

$$g_8 = \sum_k \max(0,\ T_j^k(T_m, \Omega_m) - 125°) \leq 0 \quad (77)$$

where T_j^k denotes the temperature on semiconductor junctions for k^{th} cycle point. Moreover, to avoid excessive harmonic voltage content, the inverter switching frequency has to be higher than the maximum motor frequency (a factor 20 is chosen), which leads in the following relation

$$g_9 = \sum_k \max(0, 20\omega - 2\pi F_{switch}) \leq 0 \quad (78)$$

Two additional constraints are relative to the battery cells. As underlined above, a minimum state of charge (i.e. 20%) in each accumulator cell has to be guaranteed to avoid the falling of the corresponding cell voltage to below its technological limit.

$$g_{10} = \sum_k \max(0, 0.2 - SOC_k) \leq 0 \quad (79)$$

On the other hand, the battery must provide sufficient power to the motor (taking into account all losses in the cell resistances) to fulfill the driving cycle. This leads to the following constraint

$$g_{11} = \sum_k B_k(T_m, \Omega_m) \quad (80)$$

where $B_k(T_m, \Omega_m) = 0$ if the accumulator cells are able to furnish the required current I_{bat} and $B_k(T_m, \Omega_m) = 1$ if not. Finally, the last constraint related to the reducer and ensures that it is not subject to torque values higher than its sizing torque during the driving cycle:

$$g_{12} = \sum_k \max(0, T_m - T_{red}) \leq 0 \quad (81)$$

According to the constraint handling strategy previously presented in section III.5, the constraints of the third level are not computed if some constraints of the first (or the second) level are not fulfilled. In this case, the complete simulation of the vehicle on this course can be avoided. Note also that fulfilled constraints are always set to zero to give preference to objective minimization for feasible solutions.

V.3. PEV Optimization with the NSGA-II

The optimization of the electrical traction devices of the vehicles is carried out with the NSGA-II by considering the driving cycles (road and urban cycles) previously presented. Two objectives have to be minimized i.e. the global losses in the vehicle and the embedded mass (total mass of the traction device without including the frame). The skeleton of the optimization process is shown in Fig. 19.

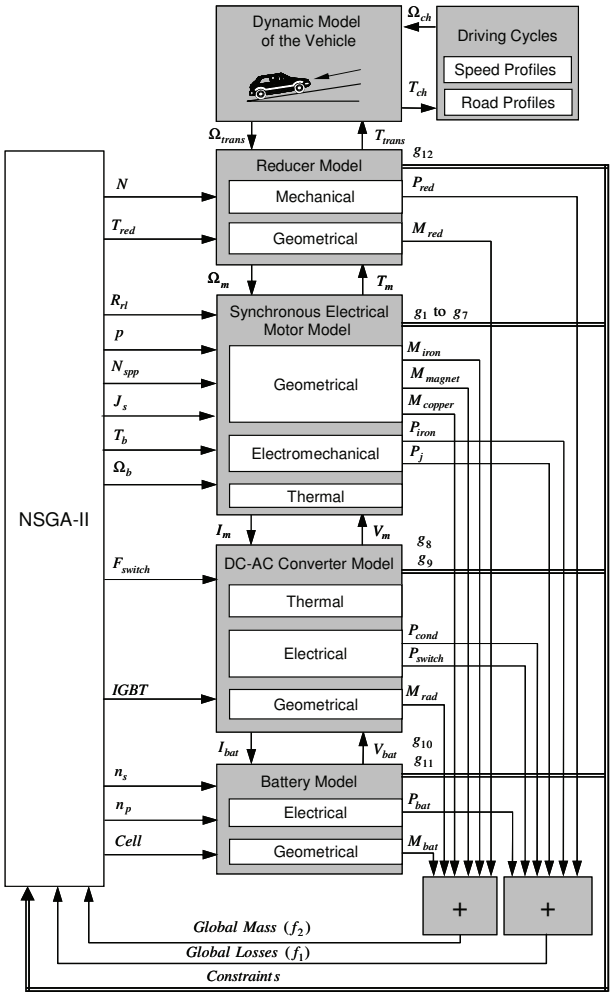

Fig. 19. The global model of PEV in the IOD process

All simulating models as well as the NSGA-II were implemented in standard ANSI C programming language. Note that the time associated to the optimization algorithm development is clearly less expensive in comparison with the time devoted to the establishment of each model and the key steps of the decision maker in the design process (i.e. choice of a relevant representation level for the system elements, suitable design variable and constraint setting). Well-known GA programming environments (e.g. GAlib [38], EO [39]) are useful for those who are not familiar with evolutionary computation. These environments can be easily associated with traditional CAD softwares.

The optimization of the electrical traction devices of the vehicles is carried out with the NSGA-II by considering the driving cycles (road and urban cycles) previously presented. The population size and the number of archive elements in the NSGA-II are set to 100. Mutation and recombination operators are similar to those presented in [21]. They are used with a crossover probability of 1, a mutation rate on design variables of 1/*m* (*m* denoting here the total number of design variables in the problem) and a mutation probability of 5% for the *X*-gene parameter used in the self-adaptive recombination scheme. The number of generations is 1500. Ten independent runs with random initial populations are performed to take account of the stochastic nature of MOGAs and in order to verify convergence and result reproducibility. Note that the CPU time necessary to evaluate feasible individual objectives approximately equals 0.25 seconds on a standard computer equipped with a 1 GHz processor. Consequently, by considering the previous control parameters (i.e. 100 individuals in the population and 1500 generations) the CPU time of the ten performed runs can vary from one to four days according to the number of feasible solutions explored during the optimization.

The global Pareto-optimal fronts obtained from these runs for the two driving cycles investigated are represented in Fig. 20. The corresponding design variable variations of Pareto-optimal solutions are given in Table V. We also illustrate in Fig. 20, the efficiency of typical "road-sized vehicles" when they are subject to the urban cycle. On the other hand, note that the "urban vehicles" energetically sized as accurately as possible are unable to comply with the more demanding road cycle in terms of power. Results show the importance of taking driving cycles into account to determine the optimal performance of PEVs.

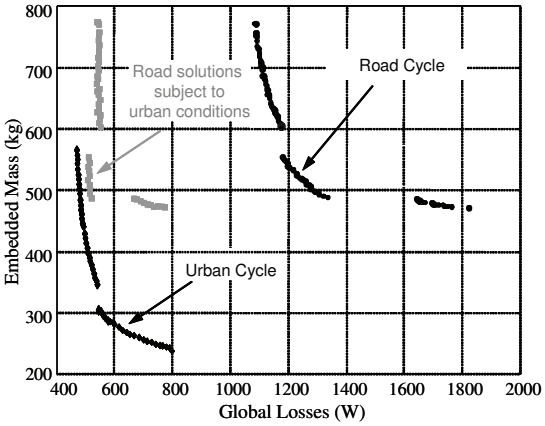

Fig. 20. PEV Pareto-optimal solutions

TABLE V
DESIGN VARIABLE RANGE OF PARETO-OPTIMAL SOLUTIONS

Design Variable	Urban Cycle		Road Cycle	
	Min	Max	Min	Max
Number of cells in series n_s	118	200	97	200
Branches in parallel n_p	1	2	2	3
Cell type	1 (39Ah)		1 (39Ah)	
Switching frequency F_{switch}	1.2	2.0	1.27	1.74
IGBT type	MII400-12E7		MII300-12E4	
Radius/length ratio R_{rl}	0.98	1.91	0.58	1.12
Number of slots/pole/phase N_{spp}	1	1	1	1
Number of pole pairs p	5	7	4	4
Current density J_s	1.31	2.15	1	1.075
Base speed Ω_b	378	644	356	412
Base torque T_b	218	387	172	196
Reducer ratio N	1	1	1	1
Sizing Torque T_{red}	No reducer (direct transmission)			

V.4. Exploitation of the IOD Process for System Analysis

IOD with MOGAs leads to the optimization of system performance by determining multiple Pareto-optimal configurations. On the other hand, the analysis of these solutions allows *a posteriori* access to valuable information associated with the system, hard to establish prior to IOD process. In particular, coupling phenomena in the system can be investigated through the study of the Pareto-optimal solution objectives in relation to the associated constraints and design variables. We briefly illustrate this point in the case of PEVs specifically sized for urban cycles

- *Partial Objective Analysis*

In the case of the urban driving cycle, the partial objective (losses and masses) evolution of the PEVs along the Pareto-optimal front is represented in Fig. 21 and Fig. 22. Note that all optimized configurations are characterized by a direct transmission (without speed reducer, i.e $N = 1$ which implies $P_{red} = 0$ and $M_{red} = 0$) and present a DC-AC converter with a negligible mass ($M_{rad} \approx 6$ kg) in comparison with other masses in the system. The partial objective analysis of Pareto-optimal solutions emphasizes the "critical" elements of the system which mainly affect global efficiency. In the case of PEVs, it can be shown in Fig 21 and Fig 22, that global objectives are mainly conditioned by both the electrical motor and the battery.

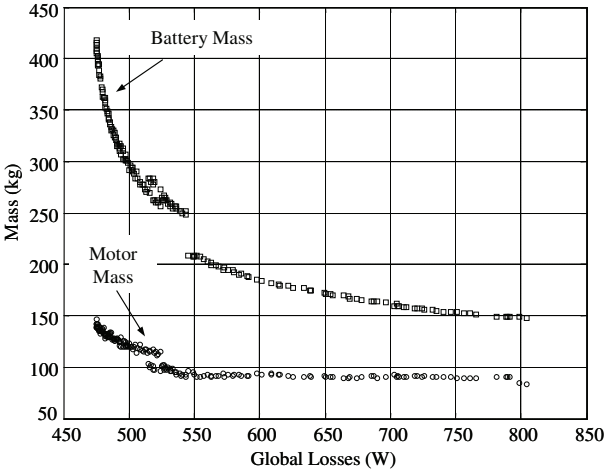

Fig. 21. Partial masses of Pareto-optimal solutions

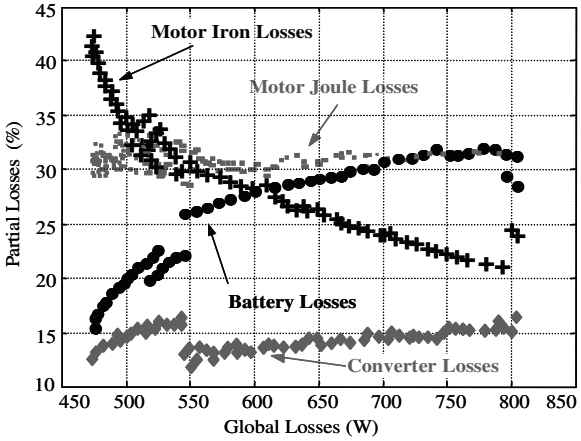

Fig. 22. Partial loses of Pareto-optimal solutions

- *Coupling analysis*

Similarly to the study of partial objectives along the Pareto-optimal front, the observation of physical variable (i.e. structural, sizing, or energetic variables as well as constraints) evolution for Pareto-optimal solutions can point out coupling phenomena in the system. For the urban driving cycle, it can be seen in Fig. 23 and Fig. 24, that the number of accumulator cells in series in the battery and the number of copper windings per slot are strongly coupled since their evolution is correlated (they present similar variations). However, in a number of cases, couplings between continuous variable are not always graphically emphasized from their evolution along the Pareto-optimal front. Therefore, we have suggested a more quantitative approach based on correlation coefficients. This approach will not be described in this paper but we invite the reader to refer to earlier publications [25], [33] for more details.

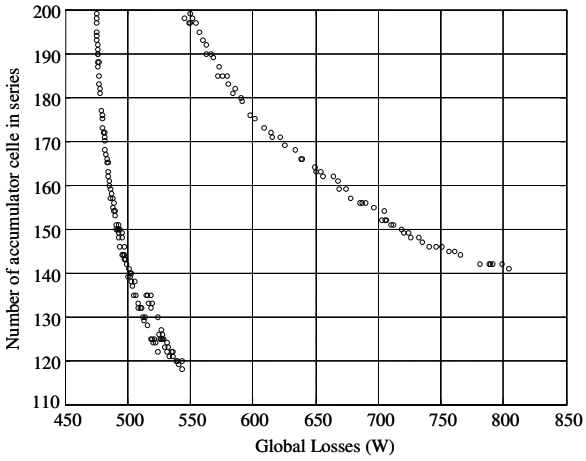

Fig. 23. Number of Accumulator Cells in Series for Pareto-optimal Solutions

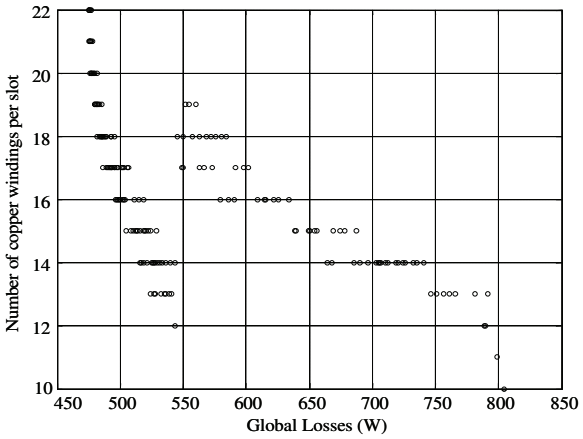

Fig. 24. Number of copper winding per slots for Pareto-optimal solutions

VI. Conclusions

In this paper, the concept of IOD for energetic systems in electrical engineering has been developed. The particularity of the optimization problems resulting from this global approach has also been underlined. The resolution of these problems notably requires the use of mixed variable and multiobjective optimization methods capable of integrating all design constraints. For that purpose, elitist MOGAs with a Pareto ranking procedure seem to be highly suitable. The interest of applying them to a real-world problem has been illustrated in the case of the traction device design for PEVs. The example considered is rather complex (7 continuous variables, 6 discrete variables, 13 constraints and 2 global objectives) and typical of the IOD approach investigated. The results obtained on this problem show the interest of using MOGAs in this context. On the one hand, they lead to the objective optimization by determining Pareto-optimal configurations, thus improving vehicle efficiency. On the other hand, they provide the designer with *a posteriori* background concerning the system. In particular critical elements in the system which mainly affect global performance can be pointed out through the study of partial objectives along the Pareto-optimal front. Moreover, couplings between design variables, constraints and objectives can be established from Pareto-optimal solution analysis. As regards future perspectives, it would be interesting to apply the IOD approach on systems with higher architecture complexity. In this context, the optimization of hybrid traction devices for electrical vehicles would be an interesting case study to examine MOGA efficiency, in comparison with other traditional design methodologies such as dynamic programming.

Acknowledgements

The authors would like to thank anonymous reviewers for their constructive comments and suggestions.

References

[1] V. Pareto, *Cours d'Economie Politique* (Lausane, 1896).
[2] C.L. Hwang, A.S. Masud, *Multiple Objective Decision Making – Methods and Applications* (Springer-Verlag, 1979).
[3] D.A. Van Veldhuizen, *Multiobjective evolutionary algorithms: classifications, analyses, and new innovations*, PhD Dissertation, Graduate School of Engineering, Air Force institute of Technology, Wright Patterson AFB, 1999.
[4] V. Chankong. Y.Y. Haimes, *Multiobjective Decision Making Theory and Methodology* (Elsevier Science Publishing Co., 1983)
[5] S.S. Rao, *Engineering Optimization – Theory and practice* (3rd edition, Wiley Interscience Publication, 1996)
[6] J.D. Schaffer, Multiple objective optimization with vector evaluated genetic algorithms, *Proceedings of the First International Conference on Genetic Algorithms and Their Applications*, Pittsburgh, 1985, pp. 93–100.
[7] J .Horn, N. Nafploitis, D.E. Goldberg, A niched Pareto genetic algorithm for multiobjective optimization, *Proceedings of the 1st IEEE Conference on Evolutionary Computation*, New Jersey, 1994, pp. 82–87.
[8] F. Kursawe, Evolution strategies for vector optimization, *Proceedings of the Tenth International Conference on Multiple Criteria Decision Making*, National Chiao Tung University, Taipei, China, 1992, pp. 187–193.
[9] P. Hajela, C.Y. Lin, Genetic search strategies in multicriterion optimal design, *Structural Optimization*, Vol. 4, pp. 99–107, 1992.
[10] B. Sareni, L. Krähenbühl, Fitness Sharing and Niching Methods Revisited, *IEEE Transactions on Evolutionary Computation*, Vol. 2, *n° 3*, pp. 97–106, 1998.
[11] D.S. Weile, E. Michielssen, D.E. Goldberg, Genetic Algorithm Design of Pareto Optimal Broadband Microwave Absorbers, *IEEE Transactions on Electromagnetic Compatibility*, Vol. 38, *n°3*, p. 518–525, 1996.
[12] J. Noble, Finding robust Texas Hold'em poker strategies using Pareto coevolution and deterministic crowding, *Proceedings of the 1st International Conference on Machine Learning and Applications (ICLMA'02)*, Las Vegas, Nevada, USA, 2002, pp. 233–239.
[13] J. Teich, T. Blickle, L. Thiele, An Evolutionary Approach to System-Level Synthesis" *Proceedings of the 5th International Workshop on Hardware/Software Codesign*, Braunschweig, 1997, pp. 167–172.
[14] C.M. Fonseca, P.J. Fleming, Genetic Algorithms for Multiobjective Optimization: Formulation, Discussion and Generalization, *Proceedings of the Fifth International Conference on Genetic Algorithms*, San Mateo, California, 1993, pp. 416–423.
[15] N. Srinivas, K. Deb, Multi-Objective function optimization using the non-dominated sorting genetic algorithm, *Evolutionary Computation*, Vol. 2, *n°3*, pp. 221–248, 1994.
[16] E. Zitzler, *Evolutionary Algorithms for Multiobjective Optimization: Methods and Applications*, PhD Dissertation, Swiss Federal Institute of Technology (ETH), Zurich, Suisse, 1999.
[17] J.D. Knowles, D.W. Corne, Approximating the nondominated front using the Pareto archived evolution strategy, *Evolutionary Computation*, Vol. 8, *n°2*, pp. 149–172, 2000.
[18] D.W. Corne, J.D. Knowles, M.J. Oates, The Pareto Envelope-based Selection Algorithm for Multiobjective Optimization, *Proceedings of the Parallel Problem Solving from Nature VI Conference*, Paris, 2000, pp. 839–848.
[19] E. Zitzler, M. Laumanns, L. Thiele, SPEA2: Improving the Strength Pareto Evolutionary Algorithm, *Evolutionary Methods for Design, Optimization and Control with Applications to Industrial Problems (EUROGEN 2001),* Athens, Greece, 2001, pp. 12–21.
[20] K. Deb, S. Agrawal, A. Pratab, T. Meyarivan, A fast-elitist non-dominated sorting genetic algorithm for multiobjective optimization: NSGA–II, *Proceeding of the Parallel Problem Solving from Nature VI Conference*, Athens, Greece, 2000, pp. 849-858.
[21] B. Sareni, J. Régnier, X. Roboam, Recombination and Self-Adaptation in Multi-objective Genetic Algorithms, *Lecture Notes in Computer Science*, Vol. 2936, pp. 115–126, 2004.
[22] C.A. Coello Coello, M. Salazar Lechuga, MOPSO: A Proposal for Multiple Objective Particle Swarm Optimization, *Congress on*

Evolutionary Computation (CEC'2002), Piscataway, New Jersey, 2002, pp. 1051–1056.
[23] X Li, A Non-dominated Sorting Particle Swarm Optimizer for Multiobjective Optimization, *Lecture Notes in Computer Science*, Vol. 2723, pp. 37–48, 2003.
[24] S. Mostaghim, J. Teich, Strategies for Finding Good Local Guides in Multi-objective Particle Swarm Optimization (MOPSO), *Intelligence Symposium Proceedings*, Indianapolis, Indiana, USA, 2003, pp. 26–33.
[25] J. Régnier, *Conception de systèmes hétérogènes en Génie Electrique par optimisation évolutionnaire multicritère*, PhD Dissertation, Institut National Polytechnique de Toulouse, 2003.
[26] D. Linden, T. Reddy, *Handbook of Batteries* (3rd edition, McGraw-Hill, 2002)
[27] J. Régnier , B. Sareni, X. Roboam, Optimal Design of Electrical engineering Systems using Pareto Genetic Algorithms, *10th International Conference on Power Electronics and Applications (EPE'2003)*, Toulouse, France, 2003.
[28] G. Slemon, X. Liu, Modeling and design optimization of permanent magnet motors, *Electrical Machines and Power Systems*, Vol. 20, pp. 71–92, 1992.
[29] E. Hoang., *Étude, modélisation et mesure des pertes magnétiques dans les moteurs à reluctance variable à double saillance*, PhD dissertation, Ecole Normale Supérieure de Cachan, 1995.
[30] R. Le Borzec, *Réducteur de vitesse à engrenages* (Techniques de l'Ingénieur, B5 640, 1999)
[31] T.D. Gillespie, *Fundamentals of vehicle dynamics* (Society of automotive engineers, 1992)
[32] R. Trigui, F. Badin, P. Maillard, A. Mailfert, Étude de l'usage réel d'un véhicule utilitaire électrique, *Revue Transport et Sécurité*, *n°50*, pp.17–32, 1996.
[33] J. Régnier, B. Sareni, X. Roboam, System optimization by multiobjective genetic algorithms and analysis of the couplings between variables, constraints and objectives, *COMPEL*, Vol. 24, *n°3*, pp. 805–820, 2005.
[34] F. Chabot, *Contribution à la conception d'un entraînement basé sur une machine à aimants permanents sans capteur sur une large plage de vitesse*, PhD Dissertation, Institut National Polytechnique de Toulouse, 2000.
[35] http://www.saftbatteries.com
[36] http://www.ixys.com/
[37] http://www.aavid.com/
[38] http://lancet.mit.edu/ga/
[39] M. Keijzer, J.J Merelo, G. Romero and M. Schoenauer, "Evolving objects: a general purpose evolutionary computation library", Evolution Artificielle (EA-01), LCNS 2310, 2001 (see also http://eodev.sourceforge.net/)

Authors' informations

* The Authors are with the LEEI, UMR INPT-ENSEEIHT/CNRS, BP 7122, 31 071 Toulouse Cedex, France (e-mail: {sareni, roboam, regnier}@leei.enseeiht.fr).

B. Sareni was born in Bron (France) in 1972. He received his Ph.D. degree in 1999 from the Ecole Centrale de Lyon. He is currently assistant professor in Electrical Engineering and Control Systems Department at the Institut National Polytechnique of Toulouse, France. He is also researcher at the Laboratory of Electrotechnics and Industrial Electronics (LEEI) of Toulouse. His research activities are related to the analysis of complex heterogeneous power devices in electrical engineering with bond graph methods and the optimization of these systems using artificial evolution algorithms.

J. Régnier was born in Blois (France) in 1975. He received his PhD degree in Electrical Engineering in 2003 from the Institut National Polytechnique of Toulouse. His work was carried out in the Laboratoire d'Electrotechnique et d'Electronique Industrielle (LEEI) and concerned the optimal design of electric vehicles using Pareto Genetic Algorithms. He is currently working as Assitant Professor at the Ecole Nationale Supérieure d'Electrotechnique, d'Electronique, d'Informatique, d'Hydraulique et de Télécommunications in the Institut National Polytechnique of Toulouse.

X. Roboam was born in Toulouse (France) in 1964. He received the Ph.D. Degree in Electrical Engineering from the Institut National Polytechnique of Toulouse in 1991. He has been in the Laboratory of Electrotechnics and Industrial Electronics (LEEI) of Toulouse since 1992 as a full-time researcher. Since 1998, he is head of the "G-EnESys" team whose the objective is to process the design problem in electrical engineering at a "system level". He develops methodologies specifically oriented towards multi-fields systems design for applications such as electrical embedded systems or renewable energy systems.